ChemPubSoc Europe

DOI: 10.1002/cbic.201700052

CHEMBIOCHEM Communications

Spectroscopic and Computational Investigations of Ligand Binding to IspH: Discovery of Non-diphosphate Inhibitors

Bing O'Dowd,[a] Sarah Williams,[b] Hongxin Wang,[c, d] Joo Hwan No,[e] Guodong Rao,[a] Weixue Wang,[e] J. Andrew McCammon,[b, f, g] Stephen P. Cramer,[c, d] and Eric Oldfield*[a]

Isoprenoid biosynthesis is an important area for anti-infective drug development. One isoprenoid target is (*E*)-1-hydroxy-2-methyl-but-2-enyl 4-diphosphate (HMBPP) reductase (IspH), which forms isopentenyl diphosphate and dimethylallyl diphosphate from HMBPP in a $2H^+/2e^-$ reduction. IspH contains a 4Fe–4S cluster, and in this work, we first investigated how small molecules bound to the cluster by using HYSCORE and NRVS spectroscopies. The results of these, as well as other structural and spectroscopic investigations, led to the conclusion that, in most cases, ligands bound to IspH 4Fe–4S clusters by η^1 coordination, forming tetrahedral geometries at the unique fourth Fe, ligand side chains preventing further ligand (e.g., H_2O, O_2) binding. Based on these ideas, we used in silico methods to find drug-like inhibitors that might occupy the HMBPP substrate binding pocket and bind to Fe, leading to the discovery of a barbituric acid analogue with a K_i value of ≈500 nM against *Pseudomonas aeruginosa* IspH.

Introduction

The enzymes IspG ((*E*)-1-hydroxy-2-methyl-but-2-enyl 4-diphosphate synthase, also known as GcpE) and IspH ((*E*)-1-hydroxy-2-methyl-but-2-enyl 4-diphosphate reductase, also known as LytB) are the last two enzymes of the 2-*C*-methyl-D-erythritol 4-phosphate (MEP) pathway of isoprenoid biosynthesis in many bacteria, as well as in some protozoa and in plants.[1] They are both 4Fe–4S cluster-containing proteins that are involved in $2H^+/2e^-$ reductions: IspG converts 2-*C*-methyl-D-erythritol-2,4-*cyclo*-diphosphate (MEcPP, **1**, Scheme 1) to (*E*)-1-hydroxy-2-methyl-but-2-enyl 4-diphosphate (HMBPP; **2**), and IspH converts **2** to dimethylallyl diphosphate (**3**) and isopentenyl diphosphate (**4**), the building blocks of isoprenoid biosynthesis. Neither enzyme is produced by humans (who use the mevalonate pathway for isoprenoid biosynthesis), but both are essential in plants and in many bacteria and protozoa, so IspG and IspH are of interest as potential herbicide or drug targets. In earlier work,[2] we reported the first structure of an IspH, from *Aquifex aeolicus* (PDB ID: 3DNF), finding that one Fe atom in the cluster was lost during crystallization, and similar results were reported for IspH from *Escherichia coli* (PDB ID: 3F7T).[3] However, using computational modeling to re-add the unique fourth Fe, together with computational docking of HMBPP substrate **1**, we were able to produce[1,2] ligand-bound structures that were very similar to later 4Fe–4S IspH/**1** X-ray structures,[4,5] and these structures led to detailed mechanism of action models[6–8] for IspH catalysis. In other early work, we discovered, based on previous reports that alkynes could bind to and be reduced by 4Fe–4S clusters,[9,10] that alkyne diphosphates such as propargyl diphosphate (**5**, PPP) were low-micromolar inhibitors of IspH (as well as of IspG, which also contains a 4Fe–4S cubane-like structure).[1] Plus, the 1-amino (**6**) and 1-thio (**7**) analogues of HMBPP were found to inhibit IspH with K_i values of 20–50 nM,[11,12] and we[13] and others reported their X-ray structures (PDB IDs: 3ZGL, 3ZGN), which are basically the same as those found with the HMBPP substrate, with N,S binding to the unique fourth Fe. We also reported[14] several other IspH–ligand complex structures, in each case with a single O-containing ligand (alcoholate or enolate) bound to the unique, fourth Fe atom with Fe–O bond lengths of ≈2 Å. What has been (and still is) missing is the X-ray structure of a ligand-free IspH—either reduced ($[Fe_4S_4]^+$) or oxidized ($[Fe_4S_4]^{2+}$)—the problem being that it has not been possible to crystallize the 4-Fe-containing protein. However, the results of ^{57}Fe Mössbauer spectroscopy[15] indicated the presence of a 5- or 6-coordinate fourth iron in ligand-free oxidized IspH, with three clusters and most likely three additional N/O ligands bound to the fourth Fe. More recently, Faus et al.[16] reported a nuclear resonant vibrational spectroscopy (NRVS) investigation of oxidized IspH and suggested that the three noncluster ligands were

[a] B. O'Dowd, G. Rao, Prof. Dr. E. Oldfield
Department of Chemistry, University of Illinois
600 South Mathews Avenue, Urbana, IL 61801 (USA)
E-mail: eoldfiel@illinois.edu
eo@chad.scs.uiuc.edu

[b] S. Williams, Prof. Dr. J. A. McCammon
Department of Chemistry and Biochemistry,
University of California at San Diego
La Jolla, CA 92093 (USA)

[c] Dr. H. Wang, Prof. Dr. S. P. Cramer
Department of Chemistry, University of California
1 Shields Avenue, Davis, CA 95616 (USA)

[d] Dr. H. Wang, Prof. Dr. S. P. Cramer
Lawrence Berkeley National Laboratory
1 Cyclotron Road, Berkeley, CA 94720 (USA)

[e] J. H. No, W. Wang
Center for Biophysics and Computational Biology
607 South Mathews Avenue, Urbana, IL 61801 (USA)

[f] Prof. Dr. J. A. McCammon
Howard Hughes Medical Institute, University of California at San Diego
La Jolla, CA 92093 (USA)

[g] Prof. Dr. J. A. McCammon
National Biomedical Computation Resource,
University of California at San Diego
La Jolla, CA 92093 (USA)

Supporting information for this article can be found under: http://dx.doi.org/10.1002/cbic.201700052.

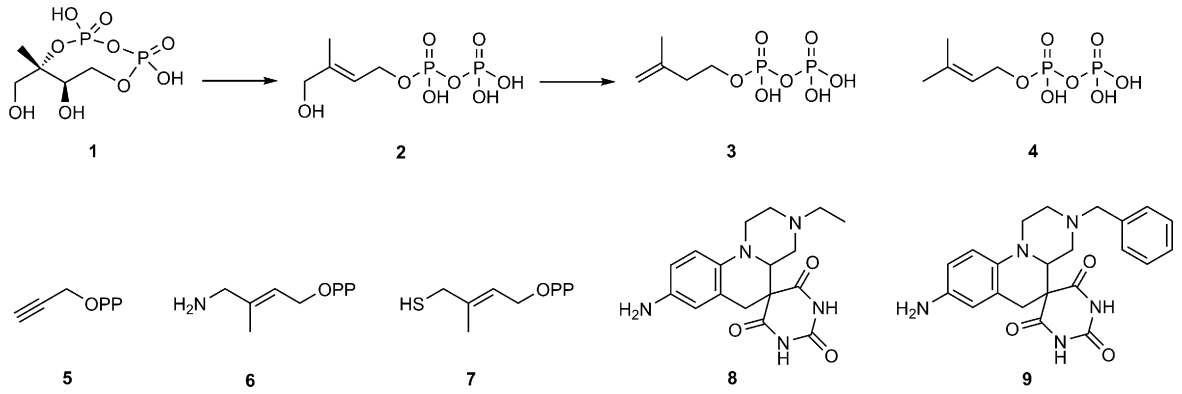

Scheme 1. Structures of IspG (GcpE) and IspH (LytB) substrates, reaction products, and ligands/inhibitors of interest. OPP = diphosphate in **5**–**7**.

H_2O molecules (or presumably OH^-, or a mixture of both). This structure is surprisingly labile, leading to loss of the fourth Fe under crystallization conditions. Ligand-free IspH is also very sensitive to O_2, whereas HMBPP and PPP, as well as an enolate-liganded species, are much less sensitive to cluster degradation by O_2,[17] suggesting that the presence of relatively bulky ligand side chains might block the H_2O/O_2 binding that leads to lability. For example, in the PPP (**5**) structure (crystallized from oxidized IspH), there is a single H_2O (or OH^-) bound to the fourth Fe,[14] whereas the acetylene group is ≈3.6 Å from the Fe, acting perhaps as a barrier to water and oxygen ligands.

In our electron paramagnetic resonance (EPR) spectroscopy work on reduced IspH–**5**, we concluded (based in part on early observations of Fe_4S_4-acetylene interactions) that there could be π-bonding with the fourth Fe in the reduced cluster, but with oxidized IspH, $S = 0$, so the system is not accessible by EPR and it is not clear if there is any alkyne interaction with the cluster. We thus used NRVS to investigate the IspH–**5** system. In addition, we used hyperfine sublevel correlation spectroscopy (HYSCORE) to investigate how another small ligand, CN^-, might bind to reduced IspH, which is of interest because CN^- can be involved in π/back-bonding with d-orbitals. The results of these experiments, together with an examination of numerous IspH and IspG structures, suggested the importance of η^1 σ-bonding of ligands to the fourth Fe, together with the presence of a bulky side chain, for IspH inhibition. We therefore performed in silico screening of possible inhibitors, finding interesting new drug-like leads that, we propose, bind in this manner.

Results and Discussion

We first investigated the interactions of IspH with alkyne diphosphate **5**, as well as with a small molecule ligand, CN^-, to see if there were any interactions of the alkyne with the cluster and whether the anionic CN^- species bound, because in principle, both might be involved in metal–ligand π-bonding/back-bonding. Then, using information from these and other related studies, we used in silico screening to identify new, drug-like inhibitor leads.

NRVS spectroscopy of the IspH–5 complex

NRVS provides ^{57}Fe-specific information on the partial vibrational density of states (PVDOS) for Fe-X vibrational modes in a molecule.[18] For systems containing 4Fe–4S cubane-like clusters, such as IspH, there are typically four main NRVS features, as shown schematically in Figure 1A:[18–21] cluster torsional

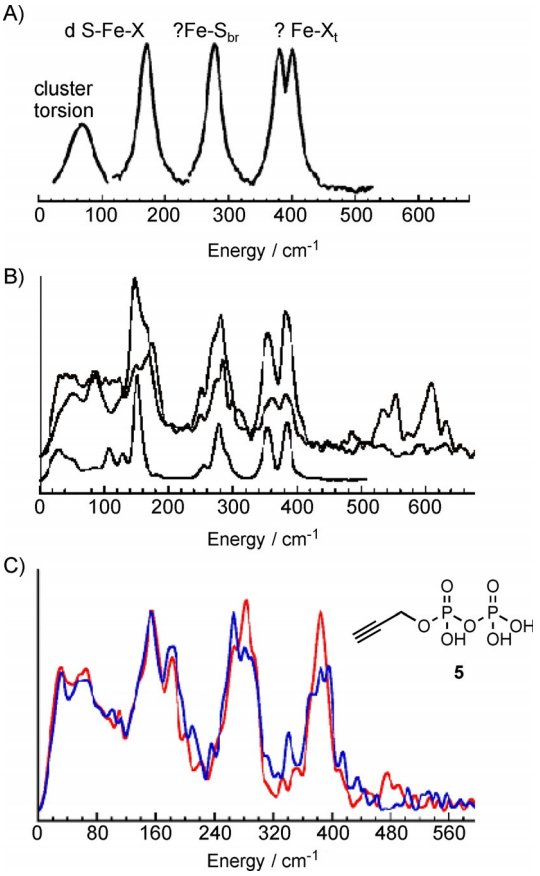

Figure 1. NRVS spectra. A) Cartoon representation of a NRVS spectrum of a 4Fe–4S cluster containing σ-bonding ligands (e.g., OR, NHR, SR, Cl) at a fourth, unique Fe-site. B) Experimental spectra of oxidized *P. furiosus* D14C ferredoxin (PfFd; black), PfFd + NO (red), and $[Fe_4S_4Cl_4](Ph_4P)_2$ (grey). C) EcIspH + **5** (red) and [^{13}C]-**5** (black).

modes occur at $<100\ cm^{-1}$, δ (S-Fe-X) bending modes at $\approx 150\ cm^{-1}$, ν (Fe–S) (cluster) stretching modes at $\approx 280\ cm^{-1}$, and ν (Fe–S_{ter}) (terminal) stretching modes in the ≈ 320–$370\ cm^{-1}$ range. Although there are, of course, additional mixed modes, these NRVS spectral features are present in most—if not all—species containing 4Fe–4S, as well as 4Fe–3S clusters.[18–21] For example, the NRVS spectrum of oxidized *Pyrococcus furiosus* ferredoxin containing a D14C mutation (which has four Cys ligands; Figure 1B, black line),[20] is very similar to that seen with the model compound $[Fe_4S_4Cl_4](Ph_4P)_2$, which contains a $[Fe_4S_4Cl_4]^{2-}$ cluster in which the four terminal ligands are Cl (Figure 1B, grey line).[20] The same basic features are also seen in oxidized IspH with HMBPP (**2**), the amino analogue (**6**), or the thiol analogue (**7**) as ligands,[16] in which O, N, or S are directly bonded to the fourth Fe. In sharp contrast, these features are all less obvious (or absent) in the NRVS spectrum of IspH in the absence of **2**, **6**, or **7**.[16] In the presence of NO, the 4Fe–4S cluster in *P. furiosus* D14C ferredoxin[22] is converted to Roussin's black salt, $[Fe_4S_3(NO)_7]^-$, and the same set of peaks (at ≈ 150, 280, and $370\ cm^{-1}$) as seen in the 4-Cys-liganded protein are present. However, there are strong additional peaks at ≈ 540 and $610\ cm^{-1}$ (red line, Figure 1B); this suggests a contribution from Fe-N-O and/or N-Fe-N vibrational modes, due in part to metal–ligand π-bonding. We thus investigated the NRVS spectra of the IspH–**5** complex to see whether there might be any evidence for an interaction between the alkyne group and the oxidized 4Fe–4S cluster (Fe–C bonding) that we previously proposed to be important in the reduced protein.

We show in Figure 1C the NRVS spectrum of EcIspH in the oxidized state ($[Fe_4S_4]^{2+}$) bound to **5** (red line). The spectrum is very similar to that seen with HMBPP (**2**) as well as with the amino (**6**) and thiol (**7**) analogues of HMBPP, bound to IspH[16], and the $[Fe_4S_4Cl_4]^{2-}$ model compound,[16] consistent with each Fe being bound to three cluster sulfurs and a single fourth atom. We also found no spectral shifts when a uniformly ^{13}C-labeled analogue of PPP (**5**) was bound to the protein (blue line, Figure 1C). These results are consistent with the presence of a single water molecule[14] binding to the fourth Fe—the tetrahedral geometry seen in the other IspH structures with **2**, **6**, and **7**[16]—with no significant bonding between the alkyne group and the cluster. A compilation of the NRVS spectra of all of the variously ligated protein and model compound 4Fe–4S cluster-containing systems discussed above, highlighting their similarities, is shown in Figure S1 in the Supporting Information. The spectra with **5** were also dissimilar to that observed with IspH containing three H_2O molecules bound to the fourth Fe, again consistent with the lack of multiple (alkyne, water) interactions with the fourth Fe.

We next sought to see how other small molecules/ions might bind to the 4Fe–4S cluster. Attempts to bind CO were unsuccessful, as determined by UV/Vis and EPR spectroscopy. However, in previous work[23] we showed that CN^- bound to reduced IspH, yielding an EPR spectrum characterized by g values of 2.08, 1.94, and 1.93 (with a small shoulder at $g=2.05$[23]), but the number of ligands, as well as their binding mode, were unknown. We thus collected HYSCORE spectra using $[^{13}C^{15}N]^-$ bound to *E. coli* IspH. As can be seen in Figure 2A, there are clearly HYSCORE features that are consistent with binding of a single CN^- to the unique, fourth Fe in the cluster. Using the EasySpin program,[24] we simulated hyperfine coupling tensors of $A(^{13}C)=[-3.9, -3.8, 0.1]$ MHz, Figure 2B, and $A(^{15}N)=[1.1, 1.1, 2.3]$ MHz, Figure 2C. Interestingly, the g values observed[23] in the EPR spectrum of IspH·CN ($g=2.08$, 1.94, 1.93) are virtually identical to those found ($g=2.09$, 1.94, 1.93) for CN^- bound to *Shewanella oneidensis* HydG (minus the "dangler Fe"[25] involved in formation of the $[Fe(CO)_2CN]$ synthon in hydrogenase function). Moreover, the HYSCORE spectrum of $[^{13}CN]$-SoHydG had a ^{13}C isotropic hyperfine coupling $A_{iso}=-2.7$ MHz, similar to the $A_{iso}=-2.9$ MHz in PfFd with bound ^{13}CN[26] and the $A_{iso}\approx 2.5$ MHz we find here. Plus, the ^{15}N HYSCORE result for $[^{13}C^{15}N]^-$ bound to SoHydG[25] was extremely similar to that we observed with IspH. So, IspH and SoHydG (the 4Fe–4S cluster), as well as the (wild-type) ferredoxin, all appeared to bind CN^- to the fourth Fe, forming a tetrahedral species. It should be noted, however, that CN^- was actually a very poor IspH inhibitor ($IC_{50}>1$ mM) and as noted by Suess et al.,[25] CN^- binds only weakly to other biological[26] as well as synthetic[27] 4Fe–4S clusters, and cysteine displaces CN^- from HydG.[25]

Ligand binding to IspH and IspG: Clues for inhibitor discovery?

Taken together, the results shown above, together with other reported work,[1] show that there are several ways that ligands

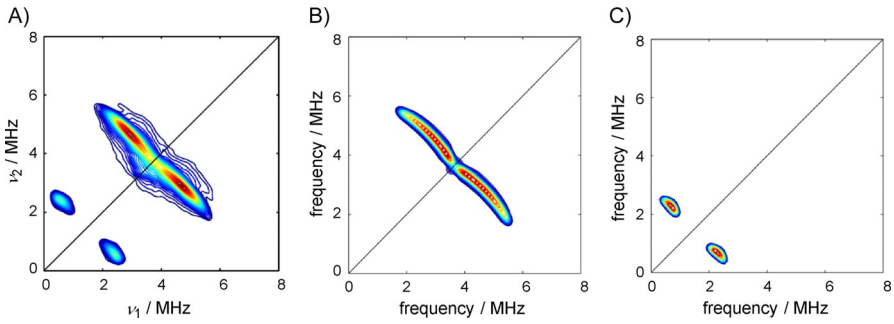

Figure 2. HYSCORE spectra of IspH·CN. A) Experimental HYSCORE spectrum of EcIspH·$^{13}C^{15}N$. Sample was reduced ($[Fe_4S_4]^+$) with dithionite. B) Simulation of ^{13}C hyperfine coupling with $A=[-3.9, -3.8, 0.1]$ MHz, Euler angle $=[0, 40\pm5, 0]^\circ$. C) Simulation of ^{15}N hyperfine coupling with $A=[1.1, 1.1, 2.3]$ MHz, Euler angle $=[0, 30\pm10, 0]^\circ$. Euler angle follows *zyz* convention.

can bind to IspH and suggest a potential route to finding new inhibitors: 1) Most ligands bind with η^1 coordination, with O, N, and S binding through σ-interactions with the fourth Fe; 2) Potential π-bonding species (CN^-, CO, propargyl alcohol) do not bind strongly; 3) Although η^2, as well as η^3, coordination is possible,[1] these cases are rare; 4) When alkyne diphosphates bind to oxidized IspH, the main cluster interaction is with a fourth H_2O (or OH^-), with the alkyne fragment blocking addition of further H_2O molecules; 5) The diphosphate moiety must contribute in a major way to IspH inhibition, because propargyl alcohol itself is a very weak inhibitor ($K_i > 10$ mM); 6) These general patterns of ligand binding are very similar in IspH and in IspG. This is shown in Figure 3A, in which we compared PPP (**5**) binding to IspH and IspG. In both cases, there is a fourth H_2O bound to the unique, fourth Fe ($d_{Fe\text{-}O} = 1.9$ Å), whereas the alkyne is more distant ($d \approx 3.6$ Å). The IspH–**5** structure is very similar to the structures found with the amino (**6**) and thiol (**7**) HMBPP analogues, with the IspH–**5** water molecule in the same position as the **6** and **7** NH_2 and SH groups, respectively, and the diphosphate groups of these structures also overlap (Figure 3B). The IspH–**5** water colocates with the ligand-bound oxygen in the IspG-MEcPP (**1**) 1st reaction intermediate[28] (Figure 3C), and the IspG–**5**-bound water is in the same position as a carboxylate oxygen in Glu307 in IspG (Figure 3D). So, in the vast majority of cases, the fourth Fe has a tetrahedral coordination geometry with O, N, or S binding to Fe. Unfortunately, these potent diphosphate-containing inhibitors are not active in cells, presumably because the diphosphate groups are very highly charged, reducing cell penetration. These observations led us to try and find more lipophilic, drug-like species that might bind to Fe, while also occupying the relatively large substrate-binding pocket.

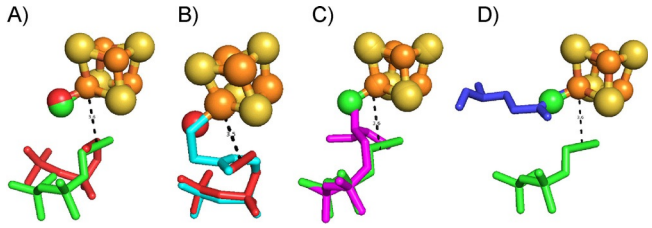

Figure 3. Comparisons between IspH/IspG structures with various ligands binding to the unique fourth Fe site. A) PPP (**5**) bound to EcIspH (red) and EcIspG (green; PDB IDs: 3URK, 4S3E). B) Superimposition of EcIspH PPP (**5**)/H_2O (red) and thiolate (cyan, **7**) X-ray structures (PDB IDs: 3URK, 4H4E). C) Superimposition of PPP (**5**)/H_2O IspG (green) structures with PPP (**5**)/H_2O-GcPE reaction intermediate structures (magenta) (PDB IDs: 4S3B, 4S3E). All structures contain a σ-bonding ligand (H_2O, RNH_2, RSH, enolate) at the unique fourth Fe structure. Binding of three water molecules to the fourth Fe leads to low stability; a water molecule and a bulky ligand that prevents binding of additional water molecules leads to more stable species. D) Superimposition of Glu307 from AaIspG (blue) and PPP (**5**)/H_2O-GcPE structures (green; PDB IDs: 3NOY, 4S3E).

Therefore, we next used an in silico approach to screen a library of drug-like compounds from the ZINC and NCI libraries, against both *Aquifex aeolicus* IspH (PDB ID: 3DNF) and *E. coli* IspH (PDB ID: 3F7T). In both cases, the fourth Fe was reconstituted computationally as described previously,[2] and we used Glide docking,[29] again as described previously.[30] Using this approach, we obtained and tested 15 potential hits (Figure S2) that were commercially available, for IspH inhibition. Fourteen out of the 15 compounds were inactive ($IC_{50} > 1$ mM), but compound **8** was active. We then obtained 11 commercially available analogues of **8** (Figure S3) and tested them against *E. coli* IspH and *Pseudomonas aeruginosa* IspH, both organisms (unlike *A. aeolicus*) being important pathogens. The most active compounds were **8** and **9**, with **8** having a K_i value of 500 nM against *P. aeruginosa* IspH (Figure 4A), and benzyl ana-

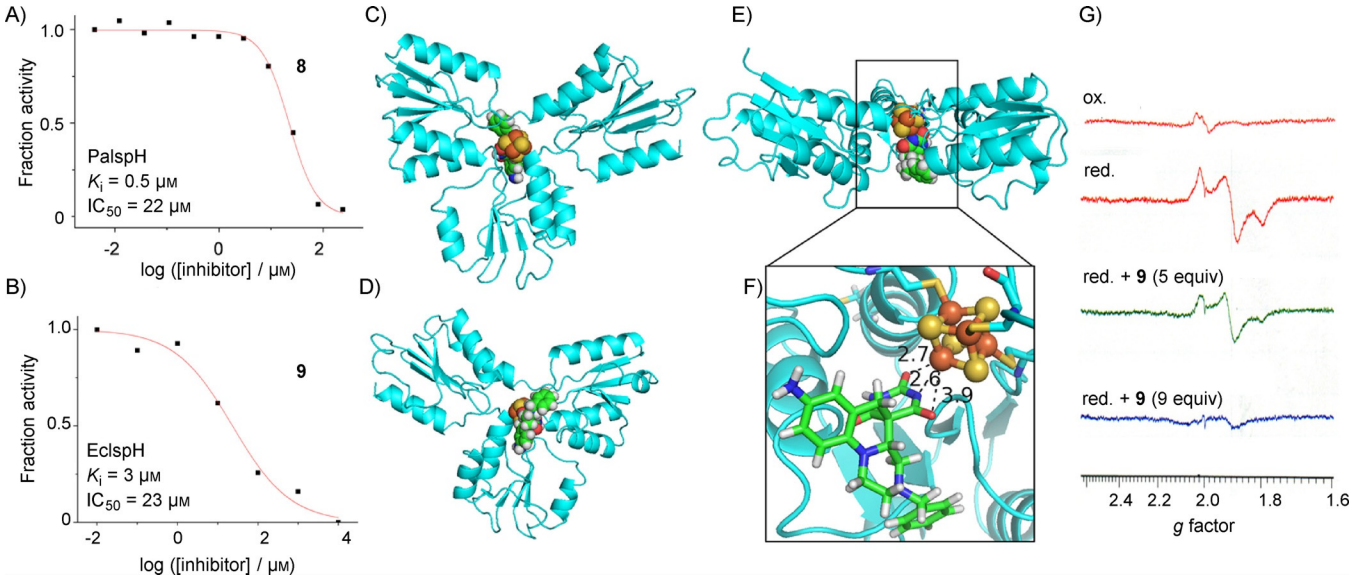

Figure 4. IspH inhibition by barbiturate analogues. A) and B) Dose–response curves for EcIspH inhibition. Computational docking structure of **9** binding to oxidized AaIspH. C) View from electron transfer side. D) View from substrate binding side. E) Side view. F) Proposed binding of the barbiturate enolate group in **9** to the unique, fourth Fe in the 4Fe–4S cluster in oxidized AaIspH. G) 9 GHz EPR spectra of PalspH. Oxidized protein (top, orange); dithionite reduced (red); dithionite reduced plus **9** (5 equiv, green); dithionote reduced plus **9** (9 equiv, blue).

logue **9** having a K_i value of 3 μM against *E. coli* IspH (Figure 4B). AaIspH was also inhibited by **9**, with a K_i value of 700 nM. These compounds are barbituric acid analogues that have some structural similarity to anti-infectives developed by Pharmacia[31] and are predicted to bind to the fourth Fe of the 4Fe–4S cluster. A view of the AaIspH–**9** complex (obtained by docking) from the electron-transfer side of the protein is shown in Figure 4C, a bottom view (substrate side) in Figure 4D, and a side view in Figure 4E. A close-up view of the ligand interacting with the fourth Fe in the cluster ($d_{Fe\text{-}N}$ = 2.6 Å; $d_{Fe\text{-}O}$ = 2.7 Å) is shown in Figure 4F. The ligand can clearly occupy the large substrate-binding site seen in the early X-ray structures, with the enolate form of the barbiturate reacting with the Fe, similar to the binding of related barbiturate enolates to Zn^{2+} in other metalloproteins.[32,33]

Interestingly, we were unable to obtain an EPR spectrum of **9** bound to IspH (from the pathogen *P. aeruginosa*), with ligand addition resulting in loss of signal intensity (Figure 4G), due perhaps to a shift in redox potential upon ligand binding or a change in relaxation behavior. In either case, **8** and **9** represent interesting new IspH inhibitor leads for further development, as they are far more lipophilic than diphosphates, they do not violate Lipinski's rules,[34] and they are not PAINS compounds.[35]

Conclusion

The results shown above are of interest for a number of reasons. First, we found that NRVS spectra of the alkyne diphosphate inhibitor **5** bound to oxidized IspH were very similar to those found for binding of HMBPP (**2**), as well as those for the amino and thiol analogues of HMBPP (**6** and **7**, respectively). There was no evidence for any alkyne–cluster interaction. Second, we showed (using HYSCORE) that CN^- bound to IspH (but was a very weak inhibitor), and that the EPR/HYSCORE spectra of the CN^--bound protein were very similar to those found with CN^- binding to SoHydG and *P. furiosus* ferredoxin, consistent with binding of a single cyanide in all three cases. Third, when compared with all known IspH and IspG structures, it was clear that in most cases, O-, N-, and S-bonding ligands bound to the unique fourth Fe in the cluster, forming tetrahedral geometries. Fourth, based on the results noted above, we sought to find novel IspH inhibitors that might bind to Fe in the active site that were also more drug-like than the diphosphate inhibitors. Using in silico screening, we found that barbiturate analogues **8** and **9** had K_i values of ≈0.5–3 μM, with the barbiturate enolate moiety binding, we propose, to the fourth Fe, with the hydrophobic domains occupying the substrate-binding site.

Experimental Section

Chemical synthesis

General methods: Compound **8** and its analogues were purchased from Vitas-M Laboratory (Hong Kong) and used without further purification. Compounds were analyzed by LC/MS and were >97% pure. Other compounds were procured from Sigma–Aldrich, Asinex, Enamine, the National Cancer Institute (NCI) Developmental Therapeutics Program Open Chemical Repository (dtp.cancer.gov/), or TimTec. All chemicals for the resynthesis of **9** were purchased from Sigma–Aldrich. ^{1}H NMR spectra were obtained on Varian Unity spectrometers at 400 and 500 MHz. High-resolution MS and elemental analyses were carried out in the University of Illinois Mass Spectrometry and Microanalytical Laboratories.

8-Amino-3-benzyl-2,3,4,4a-tetrahydro-1,2′*H*,6*H*-spiro[pyrazino[1,2-a]quinoline-5,5′-pyrimidine]-2′,4′,6′(1′*H*,3′*H*)-trione (9): The synthesis of **9** was based on the synthesis of a morpholine analogue[36] and is illustrated in Scheme 2. Piperazine (59 mmol, 5.09 g) was dissolved in THF (26 mL) by heating. Benzyl bromide

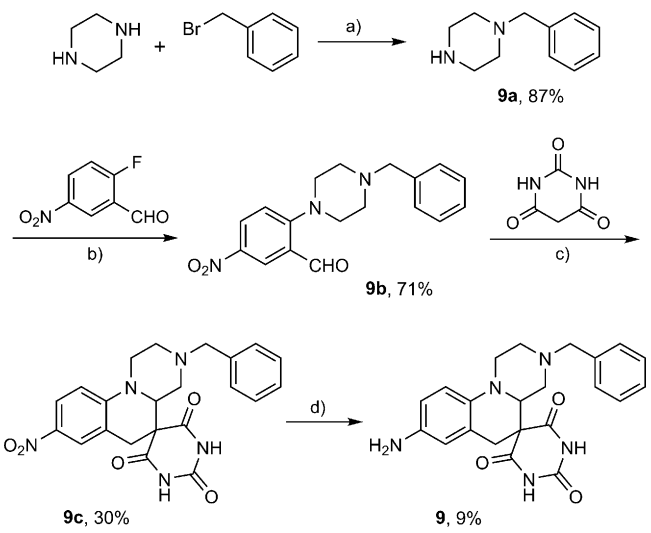

Scheme 2. Synthesis of **9**. a) THF, reflux overnight; b) NEt_3, MeCN, reflux overnight; c) MeOH, reflux overnight; d) Zn dust, AcOH, 2 h.

(8.4 mmol, 1 mL) was added dropwise to a solution of piperazine in THF under reflux. After being stirred overnight under reflux, the reaction mixture was cooled to room temperature, and the THF was removed by evaporation. The resulting residue was washed with aq. K_2CO_3 (20 mL), extracted with EtOAc (3×10 mL), washed with sat. NaCl (10 mL), dried with Na_2SO_4, and evaporated to dryness under vacuum to yield **9a** (1.29 g, 87% yield).

Compound **9a** (207 mg, 1.174 mmol) was dissolved in MeCN (3 mL) and Et_3N (1 mL). Then, 2-fluoro-5-nitrobenzaldehyde (200 mg, 1.18 mmol) was added, and the solution was stirred at reflux overnight. The reaction mixture was then diluted with EtOAc (10 mL) and washed with water (10 mL). The aqueous layer was extracted with EtOAc (2×10 mL) and dried with Na_2SO_4, then the solvent was removed under vacuum. The crude mixture was purified by column chromatography (hexanes/EtOAc, 2:1) to yield **9b** (272 mg, 71% yield).

Compound **9b** (192.77 mg, 0.592 mmol) was dissolved in MeOH (10 mL). Barbituric acid (79.76 mg, 0.623 mmol) was added to this solution, and the mixture was heated to reflux and stirred overnight. The crude reaction mixture was loaded onto a column and purified with (EtOAc/toluene, 2:3) to yield **9c** (77.33 mg, 30% yield).

Compound **9c** (30 mg, 0.069 mmol) was dissolved in 8 mL AcOH, and Zn dust (52 mg, 0.795 mmol) was added. The reaction mixture was stirred at room temperature for 2 h and then quenched with

K_2CO_3 (20 mL). Next, the mixture was diluted with EtOAc (20 mL), washed with aq. K_2CO_3 (20 mL) and sat. NaCl (20 mL), dried with Na_2SO_4, and the solvent was removed under vacuum. The crude mixture was purified by preparative TLC (100% EtOAc) to yield **9** as an orange powder (3.92 mg, 9% yield): ESI-HRMS: calcd: 406.1879, found: 406.1868 $C_{22}H_{24}N_5O_3$; compound purity determined by HPLC (Phenomenex C6-Phenyl 110A, 100×2 mm, 3 μm, 250 nm, t_R = 1.5 min): 99.7%.

Sample preparation: ^{57}Fe IspHs were prepared as described elsewhere.[5] Compound **5** was described previously.[23] For EPR spectroscopy, EcIspH and PaIspH in the oxidized state ($[Fe_4S_4]^{2+}$) and in the presence of a 20-fold excess of **5** were concentrated to ≈0.3 mM by using an Amicon Ultra centrifugal device (EMD Millipore Corporation), then glycerol was added to 20% (*v*/*v*) as a glassing agent. NRVS EcIspH samples were loaded into a Lucite cuvette (internal dimensions = 10×2.5×1 mm), then frozen in liquid nitrogen.

NRVS measurements: NRVS samples (6 mM EcIspH) were attached to a cryogenic sample base connected to a liquid helium (LHe) cryostat maintained at 10 K. Spectra were recorded according to published procedures at 03-ID at the Advanced Photon Source (APS).[37] The photon flux was ≈2.5×10^9 photons s^{-} at 1.1 eV energy resolution. Delayed nuclear Fe K fluorescence was recorded with a single 1 cm^2 square avalanche photodiode. Total data acquisition time was 19 h. Data reduction was performed by using the PHOENIX software package,[38] in which the observed raw NRVS spectra were calibrated (aligned) to the nuclear resonant peak, normalized to the I0, then summed and converted to the ^{57}Fe partial vibrational density of states (PVDOS). The spectral conversion was optimized when the observed Stokes/anti-Stokes imbalance matched the imbalance calculated with the entered temperature as a variable. The real sample temperature obtained by using this procedure was ≈60 K.

CW-EPR/ENDOR/HYSCORE spectroscopy: All continuous wave (CW)-EPR experiments were performed on a Varian E-line 122 X-band spectrometer with an Air Products helium cryostat. Typical data acquisition parameters were: microwave frequency = 9.05 GHz; field center = 3250 G; field sweep = 1000 G; modulation frequency = 100 kHz; modulation amplitude = 5 Gauss; time constant = 32 ms; temperature = 8–20 K. HYSCORE spectra were obtained on a Bruker ElexSys E-580-10 FT-EPR EPR spectrometer equipped with an Oxford Instruments CF935 cryostat. HYSCORE used a four-pulse sequence $\pi/2_{mw}$–τ–$\pi/2_{mw}$–t_1–π_{mw}–t_2–$\pi/2_{mw}$–echo; $\pi/2_{mw}$ = 16 ns and π_{mw} = 32 ns, 128 points for both t_1 and t_2, each with 24 ns steps. Time-domain data were baseline-corrected by using a third-order polynomial, then Hamming windowed, followed by zero-filling, 2D-Fourier transformation, and symmetrization. Parameters were typically: microwave frequency = 9.65–9.72 GHz, temperature = 8–15 K, microwave power attenuation = 6.5–9 dB.

Spectral simulations: HYSCORE spectra were simulated by using the EasySpin program.[24]

In silico screening: In order to find new inhibitors, we carried out in silico screening of AaIspH and EcIspH using ZINC and National Cancer Institute (NCI) libraries and Glide docking, essentially as previously described.[30]

Acknowledgements

This work was supported by the National Institutes of Health (NIH; grants GM065307 to E.O. and GM-65440 to S.P.C.) and by the Department of Energy (DOE) Office of Biological and Environmental Research (S.P.C.). NRVS measurements were performed at the Advanced Photon Source (APS) (proposals 39192/ 43032) and at SPring-8 (2015B1134). The APS is supported by the DOE Office of Basic Energy Sciences. The EPR instrumentation was supported by NIH grants S10-RR15878 and S10-RR025438. Work at University of California San Diego (UCSD) was supported by NIH, National Science Foundation (NSF), Howard Hughes Medical Institute (HHMI), National Biomedical Computation Resource (NBCR), and San Diego Supercomputer Center (SDSC). W.W. was supported by a Predoctoral Fellowship from the American Heart Association, Midwest Affiliate (award 10PRE4430022). We would like to thank Drs. Jiyong Zhao, Michael Hu and Esen E. Alp at APS for assistance with the NRVS measurements, and Mark J. Nilges for assistance with the EPR measurements.

Conflict of interest

The authors declare no conflict of interest.

Keywords: HYSCORE · in silico · isoprenoid · IspH · NRVS

[1] W. Wang, E. Oldfield, *Angew. Chem. Int. Ed.* **2014**, *53*, 4294–4310; *Angew. Chem.* **2014**, *126*, 4382–4399.
[2] I. Rekittke, J. Wiesner, R. Rohrich, U. Demmer, E. Warkentin, W. Xu, K. Troschke, M. Hintz, J. H. No, E. C. Duin, E. Oldfield, H. Jomaa, U. Ermler, *J. Am. Chem. Soc.* **2008**, *130*, 17206–17207.
[3] T. Gräwert, F. Rohdich, I. Span, A. Bacher, W. Eisenreich, J. Eppinger, M. Groll, *Angew. Chem. Int. Ed.* **2009**, *48*, 5756–5759; *Angew. Chem.* **2009**, *121*, 5867–5870.
[4] T. Grawert, I. Span, W. Eisenreich, F. Rohdich, J. Eppinger, A. Bacher, M. Groll, *Proc. Natl. Acad. Sci. USA* **2010**, *107*, 1077–1081.
[5] I. Span, T. Grawert, A. Bacher, W. Eisenreich, M. Groll, *J. Mol. Biol.* **2012**, *416*, 1–9.
[6] W. Wang, K. Wang, I. Span, J. Jauch, A. Bacher, M. Groll, E. Oldfield, *J. Am. Chem. Soc.* **2012**, *134*, 11225–11234.
[7] C. A. Citron, N. L. Brock, P. Rabe, J. S. Dickschat, *Angew. Chem. Int. Ed.* **2012**, *51*, 4053–4057; *Angew. Chem.* **2012**, *124*, 4129–4133.
[8] J. Li, K. Wang, T. I. Smirnova, R. L. Khade, Y. Zhang, E. Oldfield, *Angew. Chem. Int. Ed.* **2013**, *52*, 6522–6525; *Angew. Chem.* **2013**, *125*, 6650–6653.
[9] R. S. McMillan, J. Renaud, J. G. Reynolds, R. H. Holm, *J. Inorg. Biochem.* **1979**, *11*, 213–227.
[10] K. Tanaka, M. Nakamoto, M. Tsunomori, T. Tanaka, *Chem. Lett.* **1987**, *16*, 613–616.
[11] K. Janthawornpong, S. Krasutsky, P. Chaignon, M. Rohmer, C. D. Poulter, M. Seemann, *J. Am. Chem. Soc.* **2013**, *135*, 1816–1822.
[12] A. Ahrens-Botzong, K. Janthawornpong, J. A. Wolny, E. N. Tambou, M. Rohmer, S. Krasutsky, C. D. Poulter, V. Schünemann, M. Seemann, *Angew. Chem. Int. Ed.* **2011**, *50*, 11976–11979; *Angew. Chem.* **2011**, *123*, 12182–12185.
[13] I. Span, K. Wang, W. Wang, J. Jauch, W. Eisenreich, A. Bacher, E. Oldfield, M. Groll, *Angew. Chem. Int. Ed.* **2013**, *52*, 2118–2121; *Angew. Chem.* **2013**, *125*, 2172–2175.
[14] I. Span, K. Wang, W. Wang, Y. Zhang, A. Bacher, W. Eisenreich, K. Li, C. Schulz, E. Oldfield, M. Groll, *Nat. Commun.* **2012**, *3*, 1042.
[15] M. Seemann, K. Janthawornpong, J. Schweizer, L. H. Bottger, A. Janoschka, A. Ahrens-Botzong, E. N. Tambou, O. Rotthaus, A. X. Trautwein, M. Rohmer, *J. Am. Chem. Soc.* **2009**, *131*, 13184–13185.

[16] I. Faus, A. Reinhard, S. Rackwitz, J. A. Wolny, K. Schlage, H. C. Wille, A. Chumakov, S. Krasutsky, P. Chaignon, C. D. Poulter, M. Seemann, V. Schunemann, *Angew. Chem. Int. Ed.* **2015**, *54*, 12584 – 12587; *Angew. Chem.* **2015**, *127*, 12771 – 12774.
[17] G. Rao, E. Oldfield, *Biochemistry* **2016**, *55*, 4119 – 4129.
[18] H. Wang, E. E. Alp, Y. Yoda, S. P. Cramer in *Methods in Molecular Biology, Vol. 1122: Metalloproteins: Methods and Protocols* (Eds.: J. C. Fontecilla-Camps, Y. Nicolet), Humana, Totowa, **2014**, pp. 125 – 137.
[19] L. Lauterbach, H. Wang, M. Horch, L. B. Gee, Y. Yoda, Y. Tanaka, I. Zebger, O. Lenz, S. P. Cramer, *Chem. Sci.* **2015**, *6*, 1055 – 1060.
[20] D. Mitra, V. Pelmenschikov, Y. Guo, D. A. Case, H. Wang, W. Dong, M.-L. Tan, T. Ichiye, F. E. Jenney, M. W. W. Adams, Y. Yoda, J. Zhao, S. P. Cramer, *Biochemistry* **2011**, *50*, 5220 – 5235.
[21] S. Kamali, H. Wang, D. Mitra, H. Ogata, W. Lubitz, B. C. Manor, T. B. Rauchfuss, D. Byrne, V. Bonnefoy, F. E. Jenney, M. W. W. Adams, Y. Yoda, E. Alp, J. Zhao, S. P. Cramer, *Angew. Chem. Int. Ed.* **2013**, *52*, 724 – 728; *Angew. Chem.* **2013**, *125*, 752 – 756.
[22] Z. J. Tonzetich, H. Wang, D. Mitra, C. E. Tinberg, L. H. Do, F. E. Jenney, M. W. W. Adams, S. P. Cramer, S. J. Lippard, *J. Am. Chem. Soc.* **2010**, *132*, 6914 – 6916.
[23] K. Wang, W. Wang, J. H. No, Y. Zhang, Y. Zhang, E. Oldfield, *J. Am. Chem. Soc.* **2010**, *132*, 6719 – 6727.
[24] S. Stoll, A. Schweiger, *J. Magn. Reson.* **2006**, *178*, 42 – 55.
[25] D. L. M. Suess, I. Bürstel, L. De La Paz, J. M. Kuchenreuther, C. C. Pham, S. P. Cramer, J. R. Swartz, R. D. Britt, *Proc. Natl. Acad. Sci. USA* **2015**, *112*, 11455 – 11460.
[26] J. Telser, E. T. Smith, M. W. W. Adams, R. C. Conover, M. K. Johnson, B. M. Hoffman, *J. Am. Chem. Soc.* **1995**, *117*, 5133 – 5140.
[27] C. Zhou, R. H. Holm, *Inorg. Chem.* **1997**, *36*, 4066 – 4077.
[28] F. Quitterer, A. Frank, K. Wang, G. Rao, B. O'Dowd, J. Li, F. Guerra, S. Abdel-Azeim, A. Bacher, J. Eppinger, E. Oldfield, M. Groll, *J. Mol. Biol.* **2015**, *427*, 2220 – 2228.
[29] R. A. Friesner, R. B. Murphy, M. P. Repasky, L. L. Frye, J. R. Greenwood, T. A. Halgren, P. C. Sanschagrin, D. T. Mainz, *J. Med. Chem.* **2006**, *49*, 6177 – 6196.
[30] S. Lindert, W. Zhu, Y. L. Liu, R. Pang, E. Oldfield, J. A. McCammon, *Chem. Biol. Drug Des.* **2013**, *81*, 742 – 748.
[31] A. A. Miller, G. L. Bundy, J. E. Mott, J. E. Skepner, T. P. Boyle, D. W. Harris, A. E. Hromockyj, K. R. Marotti, G. E. Zurenko, J. B. Munzner, M. T. Sweeney, G. F. Bammert, J. C. Hamel, C. W. Ford, W. Z. Zhong, D. R. Graber, G. E. Martin, F. Han, L. A. Dolak, E. P. Seest, et al., *Antimicrob. Agents Chemother.* **2008**, *52*, 2806 – 2812.
[32] H. Brandstetter, F. Grams, D. Glitz, A. Lang, R. Huber, W. Bode, H.-W. Krell, R. A. Engh, *J. Biol. Chem.* **2001**, *276*, 17405 – 17412.
[33] P. Dunten, U. Kammlott, R. Crowther, W. Levin, L. H. Foley, P. Wang, R. Palermo, *Protein Sci.* **2001**, *10*, 923 – 926.
[34] C. A. Lipinski, F. Lombardo, B. W. Dominy, P. J. Feeney, *Adv. Drug Delivery Rev.* **2001**, *46*, 3 – 26.
[35] J. B. Baell, G. A. Holloway, *J. Med. Chem.* **2010**, *53*, 2719 – 2740.
[36] J. C. Ruble, A. R. Hurd, T. A. Johnson, D. A. Sherry, M. R. Barbachyn, P. L. Toogood, G. L. Bundy, D. R. Graber, G. M. Kamilar, *J. Am. Chem. Soc.* **2009**, *131*, 3991 – 3997.
[37] T. S. Toellner, *Hyperfine Interact.* **2000**, *125*, 3 – 28.
[38] W. Sturhahn, T. S. Toellner, E. E. Alp, X. Zhang, M. Ando, Y. Yoda, S. Kikuta, M. Seto, C. W. Kimball, B. Dabrowski, *Phys. Rev. Lett.* **1995**, *74*, 3832 – 3835.

Manuscript received: January 30, 2017
Accepted Article published: March 2, 2017
Final Article published: April 7, 2017